Poly(ethylene disulfide)/graphene oxide nanocomposites: Dynamic-mechanical and electrochemical properties

DOI: 10.1016/j.eurpolymj.2020.109694
Handle: http://hdl.handle.net/1942/33849

Poly(ethylene disulfide)/graphene oxide nanocomposites: dynamic-mechanical and electrochemical properties

Ahmad Allahbakhsh [†,*], Saeed Yari [‡,§], Mohammadhosein Safari [‡,§,ǀ], Deepak P. Dubal [ǂ]

[†]*Department of Materials and Polymer Engineering, Faculty of Engineering, Hakim Sabzevari University, Sabzevar, Iran*

[‡]*Institute for Materials Research (IMO-imomec), UHasselt, Martelarenlaan 42, B-3500 Hasselt, Belgium*

[§]*Energyville, Thor Park 8320, B-3600 Genk, Belgium*

[ǀ]*IMEC division IMOMEC, BE-3590, Belgium*

[ǂ]*School of Chemistry and Physics, Queensland University of Technology (QUT), 2 George Street, Brisbane, QLD, 4001, Australia*

*Corresponding author. Tel.: +98 51 4401 2768; E-mails: a.allahbakhsh@hsu.ac.ir, ahmad.allahbakhsh@gmail.com (A. Allahbakhsh).

Abstract

In this work, dynamic-mechanical and electrochemical properties of polyethylene disulfide and polyethylene disulfide/graphene oxide (GO) nanocomposites are investigated to explore their possible application in rechargeable batteries. The crude polyethylene disulfide, as well as GO and sodium dodecylbenzenesulfonate (SDBS) modified-GO loaded nanocomposites are synthesized through the *in situ* interfacial polymerization. The GO loaded nanocomposite presents a glass transition temperature of 4.5 °C and a high storage modulus of 115 MPa at 25 °C, which is 17% and 155% higher than that for the crude polyethylene disulfide and the SDBS-modified-GO loaded nanocomposite, respectively. Although the electrical conductivity of the

GO loaded nanocomposite is slightly higher than other two materials (due to the slightly higher electrical conductivity of GO nanosheets), the electrical conductivity of all polysulfide materials is very close and in the range of 10^{-6} and 10^{-4} S/m at low (10 Hz) and high frequencies (10^{6} Hz), respectively. Notably, the polyethylene disulfide/GO nanocomposite presents a Coulombic efficiency of 97% in a lithium cell with a conventional liquid-electrolyte.

Keywords: Nanocomposites, Polysulfides, Graphene oxide, Dynamic-mechanical properties, Flexible electrode.

1. Introduction

The concept of flexibility can be introduced in the Li-based battery technology by employing polymers as either electrodes or electrolytes [1, 2]. Compared to the elemental sulfur electrodes, organic polysulfide electrodes can present enhanced electrode kinetics [3], reduced electron-transfer resistance [4] and more importantly, pave a way to resolve the shuttle effect in lithium-sulfur batteries [5, 6]. Moreover, organic polysulfide electrodes has been widely studied as a perfect candidate for the fabrication of all-solid-state Li-batteries [7-9]. However, results available in the literature on organic polysulfide electrodes are limited to the electrochemical performance of these electrodes, and, to the best of our knowledge, no systematic study is available on the flexibility of such type of polymers.

Organic polysulfides are a class of polymeric materials with a designable backbone chain consisting of carbon and sulfur atoms [10, 11]. Such a tunable structure can present a wide range of applications from biomedical to adhesives and batteries [12, 13]. In addition to the backbone design through the polymerization process, properties of organic polysulfides can be improved through compositing these polymers with nanomaterials. However, the degree of interactions between nanomaterials and organic polysulfide matrix plays a major role in the

final performance of polysulfide-based composites and nanocomposites, especially from the viscoelastic behavior point of view [14].

Herein, dynamic-mechanical and electrochemical properties of polysulfide (PS) and polysulfide/graphene oxide (PS/GO) nanocomposites synthesized using interfacial polymerization are studied for possible applications in Li-based batteries. Although there are limited reports available on the relaxation behavior of cross-linked polysulfides [15], to the best of our knowledge, this is the first systematic investigation on the dynamic-mechanical behavior of crude polysulfides. Moreover, this is the first investigation on the role of GO nanosheets on the electrochemical properties of polysulfide electrodes. Considering literature recommendations [16], polyethylene disulfide, which is a linear polysulfide, was selected as the polymeric matrix. Moreover, based on our earlier investigations and the compatibility of consisting components [14], GO nanosheets and SDBS-functionalized GO nanosheets were selected as reinforcing nanosheets in this work. The results presented here shed a light on the applicability of viscoelastic polysulfide nanocomposites for the development of flexible rechargeable batteries.

2. Experimental

2.1. GO and GOSDBS synthesis

GO and GOSDBS nanosheets were synthesized according to the method described in details in our previous work using graphite (graphite powder, LECO) as the precursor [14]. GO nanosheets were synthesized through a modified Hummers method according to the literature [14, 17]. The product of such a process was a 1 mg/mL solution of GO nanosheets in water. To prepare GOSDBS solution, 0.5 wt.% of sodium dodecylbenzenesulfonate (SDBS, Daejung Chemicals and Metals) was added to the fabricated 1 mg/mL GO solution. These GO and

GOSDBS solutions were stable solutions of nanosheets in water and used after a centrifuge purification step for the synthesis of nanocomposites.

2.2. Synthesis of the pure PS polymer, PS/GO and PS/GO-SDBS nanocomposites

Polyethylene disulfide (PS) was synthesized through the interfacial polymerization of sodium disulfide (inorganic polysulfide, Merck) and ethylene dichloride (organic dihalide, Merck) monomers, as described in the literature [17]. In a typical synthesis process, sodium disulfide (as the aqueous monomer) was first prepared through the reaction of anhydrous sodium hydroxide (Merck) and the elemental sulfur (Merck) according to the stoichiometry required for the disulfide formation. Then, 250 mL of a 2M sodium disulfide solution was placed in a 500mL four-necked round-bottom flask equipped with a stirrer, a dropping funnel, a condenser, and a thermometer.

A magnetic stirrer was used to mix the solution at a constant stirring rate of 600 rpm and the solution was heated up to 80 °C to reach the boiling point of the ethylene dichloride. At this point, the constant temperature was maintained and 80mL of ethylene dichloride (as the organic monomer) was added dropwise to the reaction solution using a dropping funnel through one hour. After the complete addition of the organic monomer, the reaction mixture was maintained at 80 °C for another one hour under vigorous stirring to achieve polyethylene disulfide. The synthesized polyethylene disulfide color-changed to a white powder after separation and drying (see **Figure 1**). This product was labeled as PS throughout this work.

Similar synthesis procedure was followed for PS/GO and PS/GOSDBS nanocomposites [14, 18]. GO and GOSDBS solutions (1 mg/mL) were added to the 2M sodium disulfide solution to form 1 wt.% GO- and GOSDBS-sodium disulfide solutions, respectively. Using these solutions as the aqueous monomer solution in the *in situ* interfacial polymerization process, PS/GO and PS/GOSDBS nanocomposites were synthesized. The samples were further molded

using a hot press at the softening point of the PS, 80 °C [19], under 250 kg/cm^2, to prepare samples for dynamic-mechanical and electrochemical characterizations.

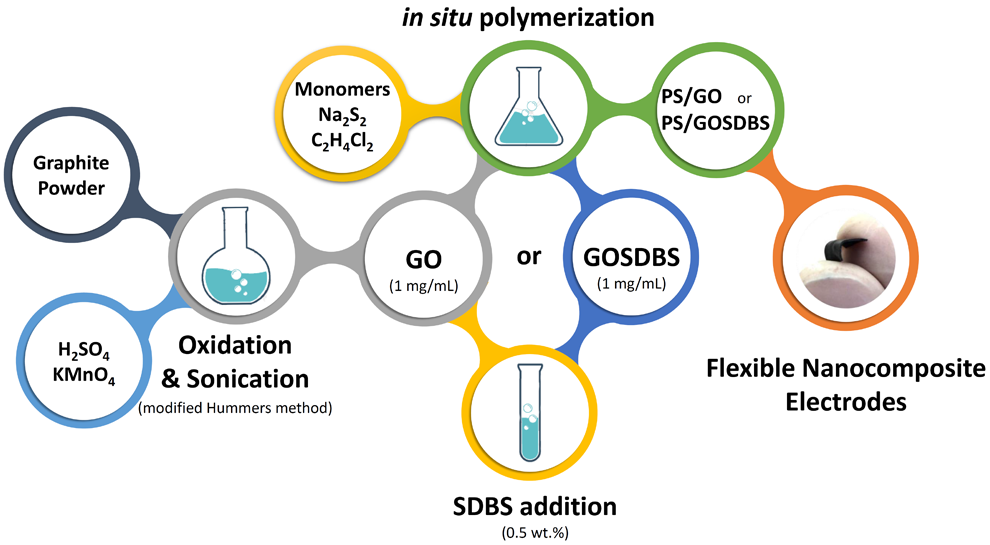

Figure 1. A schematic of the synthesis process followed for the fabrication of PS/GO and PS/GOSDBS nanocomposites

Characterizations

Atomic force microscopy (AFM) results were obtained using a Dualscope DS 95-200, DME atomic force microscope equipped with a rectangular cantilever (cantilever coating: aluminum) in the non-contact mode and with a scan rate of 20 μm/s on a freshly cleaved mica surface. A Nicolet IR100 spectrometer was used for obtaining Fourier transform infrared (FTIR) spectra of samples (ASTM E 1252-98). X-ray powder diffraction (XRD) patterns were obtained using an Inel Equinox 3000 diffractometer operated at 40 kV and 30 mA (step size: 0.02 °/s) equipped with a Cu kα (λ = 1.54056 Å) radiation source.

Dynamic mechanical analysis (DMA) were performed using a NETZSCH DMA 242 analyzer in the tension deformation mode (using a tension sample holder) and in both temperature-sweep and frequency-sweep modes. Temperature-sweep analyses were reported at a constant frequency of 5 Hz with a heating rate of 5 °C/min. Frequency-sweep analyses were recorded

at six different frequencies (i.e., 0.1, 1, 5, 10, 50 and 100 Hz) with a heating rate of 5 °C/min. The Williams-Landel-Ferry (WLF) model was used to obtain time-temperature superposition (TTS) plots. See Supporting Information for TTS plots and WLF constants of each sample.

AC electrical conductivity results were measured using GW INSTEK LCR-8101G LCR meter at room temperature (ASTM D 150-98). Transmission electron microscopy (TEM) results were obtained with a Zeiss EM10C transmission electron microscope at an accelerating voltage of 80 kV. Ultra-thin sections for TEM analysis were prepared using a Reichert OMU3 ultramicrotome equipped with a diamond knife. A Tescan VEGA-II apparatus equipped with an energy beam of 20 kV was used to obtain scanning electron microscopy (SEM) results. Thermogravimetric analysis (TGA) were recorded using a Mettler Toledo TGA/SDTA 851 analyzer under N_2 atmosphere and with a heating rate of 10 °C/min.

The electrochemical activity of samples were studied using cyclic voltammetry (CV) and galvanostatic charge/discharge tests with employing a VMP3 (biologic) potentiostat/galvanostat instrument. A two-electrode 2025 coin cell with a Li counter electrode (CE) was used for all tests. The working electrodes (WE) were prepared by coating a very thin layer (< 5 mg) of each sample on an Al mesh current collector (d = 15 mm). The electrolyte was provided from Soulbrain America and Li was purchased from Sigma Aldrich. Coin cell parts used in this manuscript were obtained from MTI Co. A Celgard 2325 separator was inserted between WE and CE, and all three layers were soaked with a 1M $LiPF_6$ in EC:EMC (1:1) electrolyte. The cell assembly was performed inside an Ar-filled glove-box (Mbraun) with H_2O and O_2 concentrations < 1 ppm. The voltage range of CV tests was 0.5-4 V with a scan rate of 10 mV/s. The galvanostatic charge/discharge tests were performed at a current of 0.5 µA with discharge and charge cut-off potentials of 1 and 3 V, respectively.

3. Results and discussion

GO and GOSDBS nanosheets used in this study exhibited a multi-layered morphology with an average thickness of 2-3 nm (**Figure 2**). Considering the average thickness of a GO nanosheet (which is about 1-1.5 nm [17]), it can be concluded that GO and GOSDBS nanosheets used here for the *in situ* synthesis of nanocomposites were of approximately 2-3 layers. Moreover, FTIR studies confirmed the presence of oxygen-containing functional groups on basal plane and edges of GO nanosheets.

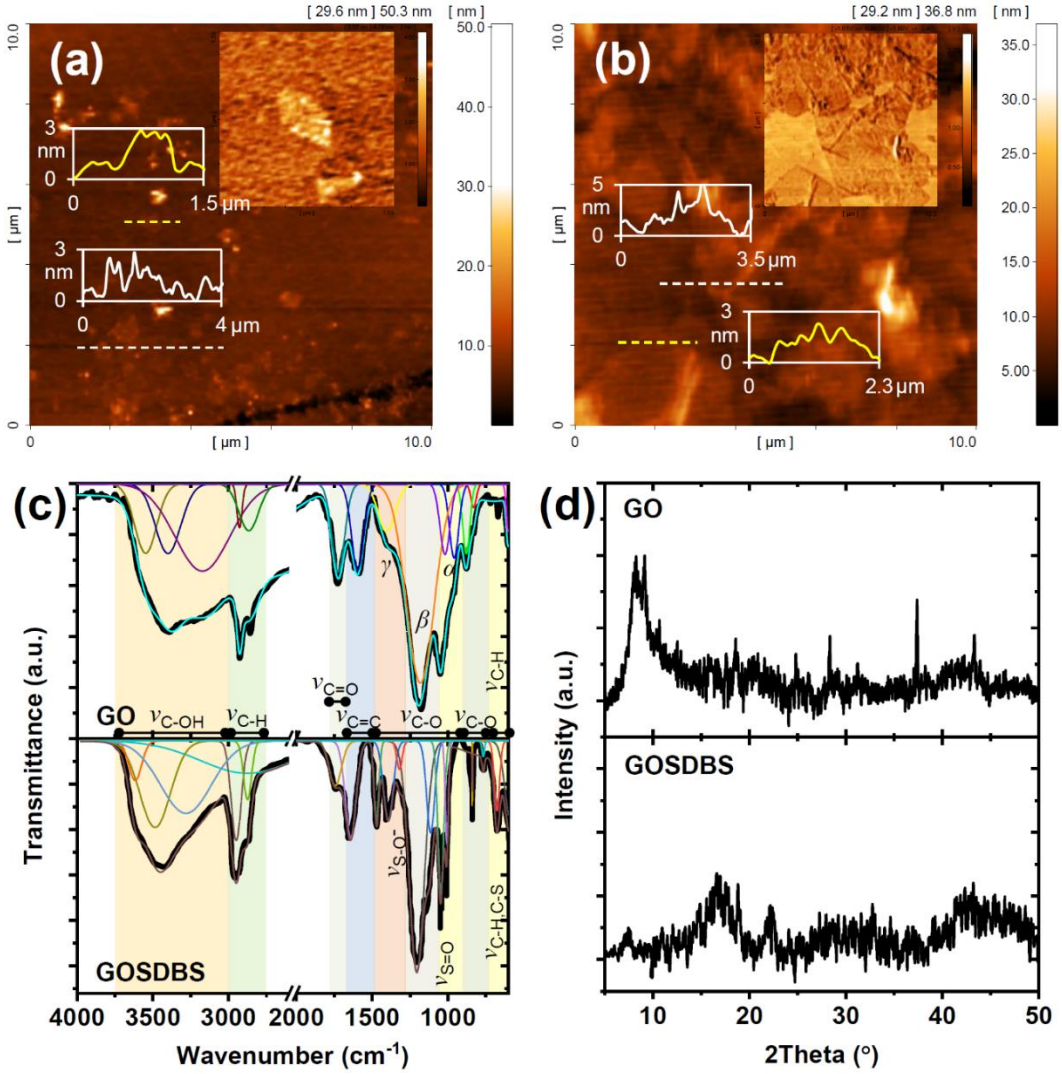

Figure 2. Characterization of GO and GOSDBS nanosheets: AFM topographic images and respective height distribution curves of (a) GO and (b) GOSDBS nanosheets (inset: AFM phase trace image) as well as (c) FTIR spectra and (d) XRD patterns of nanosheets

As discussed in the literature [14], with the intercalation of SDBS molecules into the interlayer spacing of GO nanosheets, O-moieties on basal plane and edges of GO nanosheets can form physical interactions (perhaps C–H···O hydrogen bonding [14]) with the linear hydrophobic alkane-based end of SDBS molecules (–CH_3 groups). Consequently, with a change in the surface charge of nanosheets in the presence of SDBS, the interlayer spacing of nanosheets increases. Since the peak observed in the XRD pattern of GO nanosheets (~10° in Figure 2 d) is a measure of the interlayer spacing between adjacent GO nanosheets, a shift in the 2θ value of this peak to lower values can be expected with an increase in the *d*-spacing of nanosheets [14]. Such an increase in the interlayer spacing of GO nanosheets can result in the elimination of the GO characteristic peak from the XRD pattern of GOSDBS [14]. Increased interlayer spacing of nanosheets facilitates the intercalation of polymeric macromolecules into the interlayer spacing of nanosheets and therefore, as the in situ polymerization process used here for the synthesis of nanocomposites was conducted in the aqueous phase (Figure 1), the chance for the synthesis of nanocomposites with fully exfoliated morphologies increases with an increase in the GO interlayer spacing.

Based on the nature of the polymerization process and the organic dihalide monomer used here for the synthesis of linear polysulfides, these polymers can present a wide range of structural characteristics [20]. Crude and non-plasticized polyethylene disulfide has a fascinating structure that becomes hard at around -27 °C and fairly soft at ~ 80 °C [19]. At room temperature, this elastomeric polymer presents a semi-plastic behavior, which is more like a hard plastic [19, 20]. As-synthesized PS presented a unique microstructure consisted of crystalline organic fractions in an amorphous structure (**Figure 3 a**).

This is a unique structure for an elastomeric material, which can be identified in the microstructural characterizations of this material with two almost-co-centered characteristic peaks at 2θ values in the range of 20-21°. The wide peak represents the amorphous nature of

the PS macromolecule and the sharp one represents the crystalline portions in the structure. It has been reported that polyethylene disulfide macromolecules can only crystallize to a small extent (~14%) [21]. Therefore, this structure mainly represents an elastomeric structure with a small extent of crystallized portions.

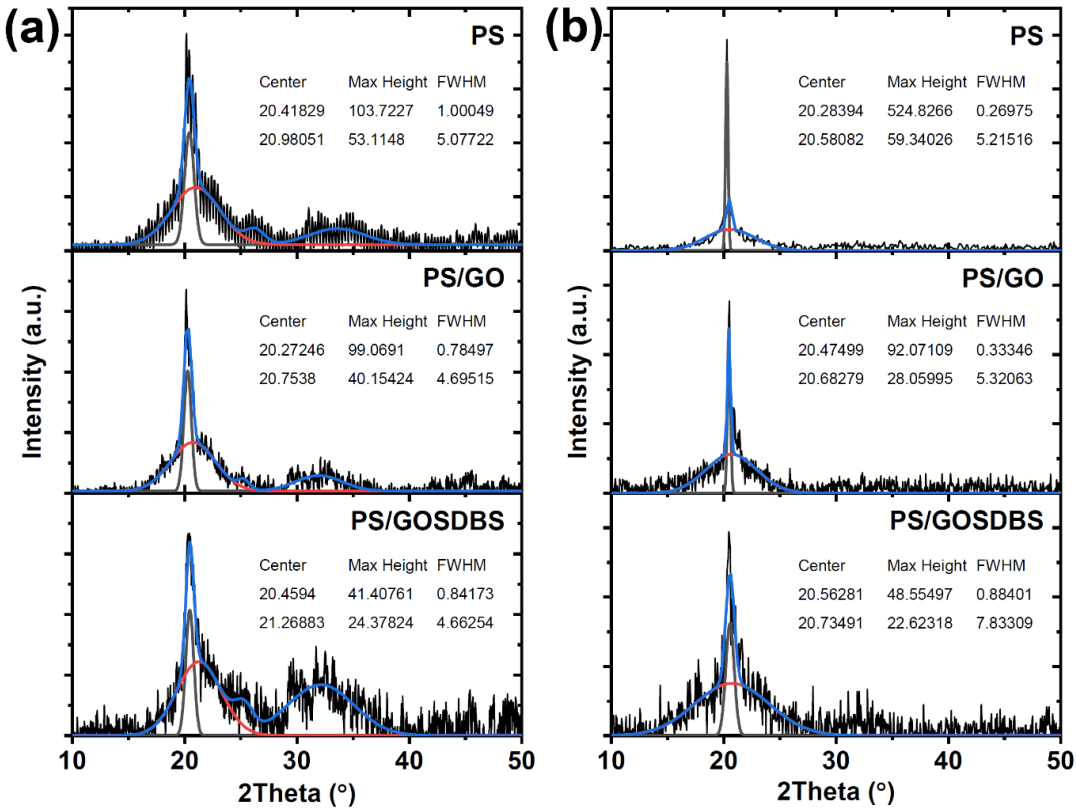

Figure 3. Structural characteristics of synthesized nanocomposites: XRD patterns of (a) as-synthesized and (b) molded samples

According to XRD studies, the incorporation of GO or GOSDBS nanosheets (see Supporting Information for the characterization of nanosheets) did not affect the microstructure of polyethylene disulfide significantly, as the full-width-at-half-maximum (FWHM) of the amorphous-related peaks in the XRD patterns of nanocomposites and the neat PS were almost identical (Figure 3 a). Moreover, no sign of GO characteristic peak (2θ~10°) was observed in the XRD pattern of nanocomposites, suggesting the formation of an exfoliated morphology in the structure (see Supporting Information for TEM results).

To see how the hot molding process may affect the structure of the crude neat PS and nanocomposite samples, XRD patterns of molded samples were also investigated (**Figure 3 b**). Upon the molding process, there was a clear increase in the intensity of the peaks associated with the crystalline phase of the crude PS. However, when GO nanosheets were incorporated in the structure, the main change between the XRD patterns of as-synthesized and molded samples was in the intensity of the peaks corresponding to amorphous-phase and consequently, the FWHM values of those peaks. The observed decrease in the maximum height of this peak in the presence of GO nanosheets can be related to the relaxation-restrictions of PS macromolecules in presence of GO, which was increased due to interactions between nanosheets and polymeric chains. However, based on XRD results, one can postulate that no significant change occurred in the structure of samples due to the molding process.

Based on experimental and theoretical investigations, the GGG'G conformation (i.e. gauche (60°), gauche (60°), gauche prime (-60°) and gauche (90°) internal rotation conformations) along the sequence of -S-CH_2-CH_2-S-S- bonds can be considered as the most possible conformation for the polyethylene disulfide [22]. Due to their unique structure, polysulfides are almost insoluble in most of organic solvents (due to the high molecular weight and sulfur content [21, 23] and interactions between adjacent polymeric chains [24]) and therefore, a clear understanding of the structure of these polymers is still missing. However, it was suggested that the hydroxyl groups should be considered as the most probable end groups for polysulfide macromolecules synthesized through the condensation polymerization of an inorganic polysulfide and an organic dihalide [21].

This structure can be further studied using FTIR investigations of polyethylene disulfide macromolecules, as shown in **Figure 4** (see Supporting Information for peak assignments). In the FTIR spectrum of the crude PS (Figure 4 a), the infrared band of S-S stretching mode can be expected at about 460-480 cm^{-1} [25]. Bands at frequencies under 750 cm^{-1} can be assigned

to C-S stretching modes; since such frequencies are too low for CH_2 rocking vibrations [22]. The overlapped CH_2 rocking frequencies of the C-C bond can be observed at 821 and 992 cm^{-1}, which corresponds to the gauche conformation around the C-C bond of polyethylene disulfide [22, 25].

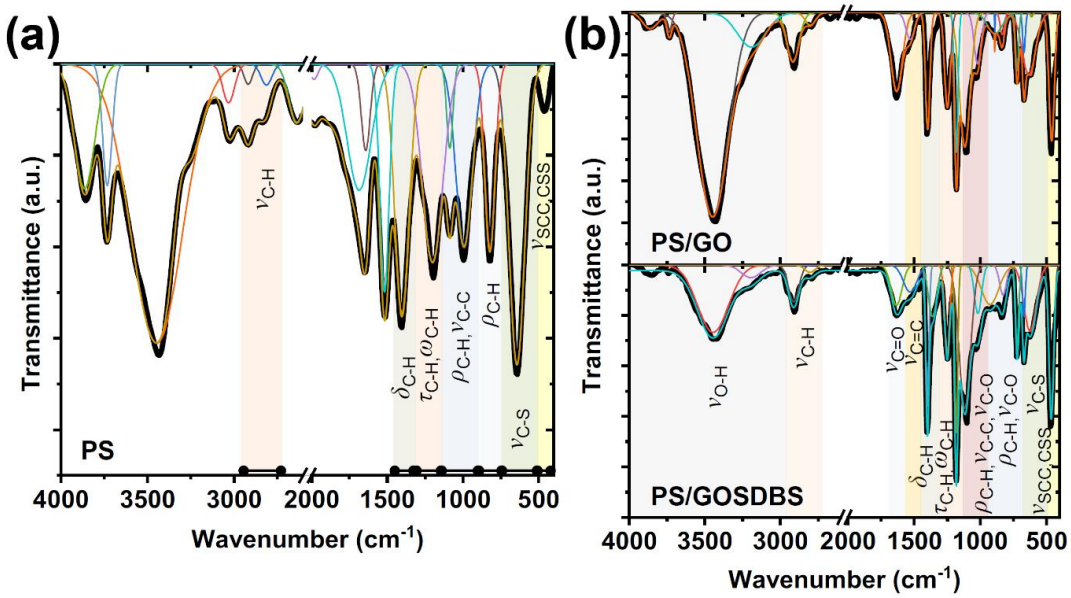

Figure 4. Surface chemistry of nanocomposites: (a) FTIR spectra of as-synthesized PS and (b) nanocomposite samples

As mentioned earlier, in their solid form, polysulfides are expected to have hydroxyl end groups. Presence of such groups can lead to high-intensity and wide bands in the FTIR spectrum of the crude PS in the region 3000-3800 cm^{-1}. However, as reported earlier using nuclear magnetic resonance (NMR) analysis, the formation of -SH end-groups through the interfacial polymerization of polyethylene disulfide can also be possible [17]. It should be noted once again that the exact structure of end-groups in the backbone of linear polysulfides is still unclear [21].

Either in the presence of GO or GOSDBS nanosheets, a clear change in the position and intensity of PS characteristic peaks can be observed (Figure 4 b). The observed change in the intensity of bands related to the hydroxyl end-groups (and the residual moisture [26]) in Figure

4 b (region 3000-3600 cm^{-1}) can be related to two simultaneous phenomena in the structure of PS with incorporating either of GO and GOSDBS nanosheets. The first phenomenon can be a significant increase in the content of hydroxyl groups in the structure of nanocomposites due to GO and GOSDBS hydroxyl groups. The second one can be hydrogen-bonding interactions between nanosheets and PS macromolecules. Such interactions may affect the structural characteristics of nanocomposites significantly, as the relaxation performance of polymeric macromolecules can be influenced in the vicinity of graphene-based nanosheets.

Compared to hydroxyl groups, carboxyl groups may not have a significant role in physical interactions between nanosheets and PS macromolecules, as bands related to the carboxyl groups on basal plane and edges of nanosheets were distinguishable in the FTIR spectra of nanocomposites. Regarding the PS/GO nanocomposite, a clear change in the intensity of bands related to the ν C-O β-region (1100-1280 cm^{-1}) and γ-region (1280-1500 cm^{-1}) can be observed in the FTIR spectra of as-synthesized nanocomposites (Figure 4 b), which can be related to the nature of interactions between GO nanosheets and PS macromolecules. It should be noted here that the molding process did not affect the structure of nanocomposites significantly; since all assigned bands of nanocomposites were also observed in the FTIR spectra of molded nanocomposites (see Supporting Information for FTIR spectra of molded nanocomposites). However, some changes in the intensity of bands were observed in the FTIR spectra of molded samples, which were expected since some changes in the structure of nanocomposites was observed through XRD studies of molded samples.

As discussed through structural studies, PS is expected to have a hard plastic-like structure at low temperatures [19, 21]. Based on the dynamic-mechanical studies (**Figure 5**), the crude PS presented a high storage modulus (E') of 1492 MPa at - 45 °C and 5 Hz. As the temperature increased, the storage modulus of the crude PS decreased with an increase in the mobility of polysulfide macromolecules. The storage modulus of the crude PS decreased to about 60 MPa

at 45 °C, the temperature that is much higher than the glass transition temperature of this disulfide polymer.

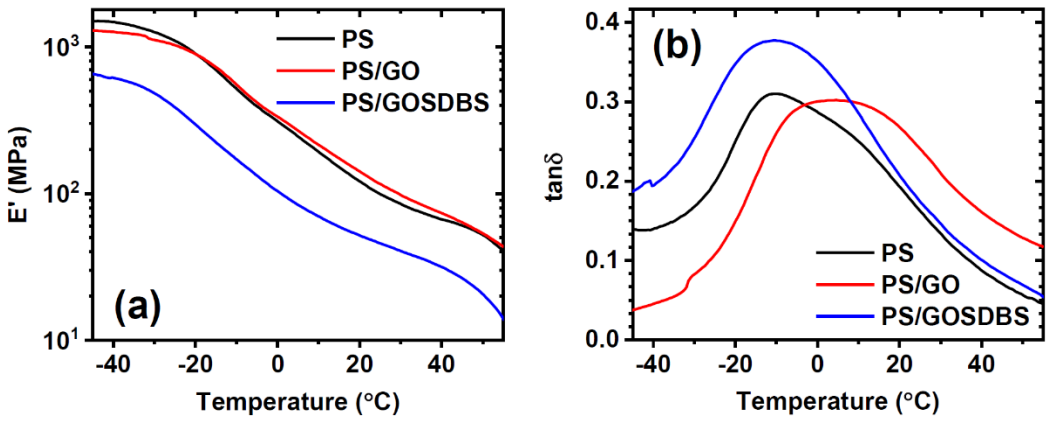

Figure 5. Dynamic-mechanical behavior of molded samples: (a) storage modulus (E'), (b) loss tangent (tanδ) curves

It is well-known that the glass transition temperature (T_g) of polysulfides depends strongly on the hydrocarbon moiety and the length of the polysulfide chain [27]. Polyethylene disulfide is expected to have a T_g of about -27 °C [27]. However, the crude polysulfide synthesized in this work using the interfacial polymerization presented a T_g of about -10 °C. Moreover, the synthesized PS shows a wide glass transition temperature range (Figure 5 b), which indicates that even at temperatures higher than the room temperature (45 °C), the structural transition of polysulfide macromolecules still develops. This is the reason for the observed unique microstructure of this polymer with crystalline portions in the structure.

With the incorporation of GO nanosheets, the dynamic-mechanical properties of PS macromolecules enhanced at temperatures higher than the glass transition region of the nanocomposite. At room temperature (25 °C), the storage modulus of the PS/GO nanocomposite was more than 115 MPa, which is higher than that of the crude PS (98 MPa). Moreover, with an increase in the temperature to ~ 45 °C, the storage modulus of the

nanocomposite was about 63 MPa. The observed limited enhancement in the dynamic-mechanical properties of the PS/GO nanocomposite at higher temperatures can be described by considering the very low content of GO nanosheets, which can slightly affect the viscosity of PS macromolecules at higher temperatures.

Unlike what expected, the incorporation of SDBS-modified GO nanosheets did not lead to any enhancement in the dynamic-mechanical properties of the system (Figure 5 a). This is most likely due to the nature of interactions between nanosheets and PS macromolecules. In case of the PS/GO nanocomposite, the formation of such interactions led to a clear change in the dynamic-mechanical properties of the system. However, in the PS/GOSDBS nanocomposite, the adverse effect was observed where the dynamic-mechanical properties degraded, which might be ascribed to the low compatibility of nanosheets and polymeric chains.

The role of interactions between PS macromolecules and nanosheets on dynamic-mechanical properties of the system can be studies using the mean of the loss tangent in the system. The loss tangent is a well-known measure of the damping in polymeric systems [28]. The value of tanδ represents the energy loss per cycle within the framework of linear viscoelasticity and therefore, indicates the damping performance of viscoelastic systems [28]. Polysulfides are a well-known class of polymers with the high ability to internally relieve stress [27]. The PS has a maximum tan δ of 0.31017 at -10 °C (Figure 5 b). This value represents a polymeric system with a medium damping performance, compared to hard-plastics with high-damping properties [28].

The position and the value of the loss tangent peak is a perfect measure for investigating the polymer/reinforcing agent in a nanocomposite system. A shift in the position of the tan δ peak to higher temperatures represents the constrained polymer chains in the structure of nanocomposite systems [29]. Moreover, a decrease in the value of tan δ is also a sign of high

interactions between polymeric macromolecules and the reinforcing material. Consequently, the shift in the tan δ peak temperature to higher temperatures (4.5 °C) and the observed decrease in the value of tan δ with incorporating GO nanosheets (0.302) confirms the formation of strong interactions between PS and GO in the PS/GO nanocomposite. Based on dynamic-mechanical studies, the incorporation of GO nanosheets resulted in the formation of improved interactions between nanosheets and PS macromolecules than GOSDBS nanosheets.

The electronic conductivity of solid sulfur is about 0.5×10^{-27} S/m at room temperature [30, 31]. Although the incorporation of carbonous materials in the formulation of sulfur electrodes can enhance the electronic conductivity, the cost of this improvement is less active material in the structure [30]. Compared to the elemental sulfur, polyorganodisulfides can present much higher electronic conductivities. Based on the nature of the polymeric backbone, polyorganodisulfides can have electronic conductivities in the range of 10^{-2}-10^{-13} S/cm [3, 32-34]. Although the lowest electronic conductivity of polyorganodisulfides is much higher than the elemental sulfur, enhancing this characteristic can still be beneficial for battery applications.

The electrical conductivity of PS was in the range of 10^{-4}-10^{-7} S/m, and frequency-dependent (**Figure 6**). The electrical conductivity in polymeric networks is expected to have a shift from a low-frequency dc plateau to a dispersive high-frequency region above a critical frequency [35]. Same behavior was observed in this study for the electrical conductivity of the crude PS sample (Figure 6 a). When GO nanosheets were incorporated, the electrical conductivity of the system slightly increased at all frequencies. However, in the case of PS/GOSDBS nanocomposite, the electrical conductivity of the system was only higher in the low-frequency range.

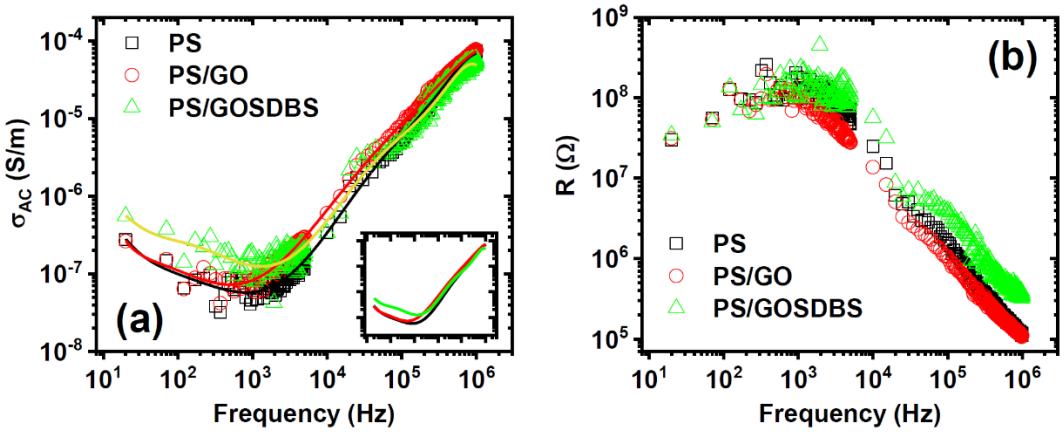

Figure 6. Electrical properties of fabricated samples: (a) AC electrical conductivity (σ_{AC}) and (b) AC resistance (R) curves of samples

Above the critical frequency and through the dispersive region, the universal power law, first presented by Jonscher ($\sigma_{AC} \propto \omega^n$, where n is the fractional exponent), can be used to describe the ac component contributing to the dispersive region [35]. The value n in this equation reflects extent of tortuosity for mobile charges [36]. Moreover, the dispersive region represents the chemical environment within the material and therefore, can be considered as an indicator for the structural properties of the material [36]. Through the dispersive region, a change in the value of n from $n \approx 1$ to $n \approx 0.9$ was observed when GO nanosheets were incorporated, which can be related to the high aspect ratio of GO nanosheets and a reduction in the carrier tortuosity with GO loading. Moreover, the electrical conductivity of the PS/GO nanocomposite was relatively higher than that of the PS/GOSDBS nanocomposite, which can be attributed to the higher extent of interactions in the PS/GO nanocomposite.

Considering higher dynamic-mechanical characteristics and electrical conductivity, one can postulate that the PS/GO nanocomposite might be a better candidate for the flexible electrode applications, compared to the PS/GOSDBS nanocomposite. Moreover, the higher electronic characteristics of the PS/GO nanocomposite in the dispersive region indicates the formation of more interactions between nanosheets and the PS matrix in this nanocomposite, compared to

the PS/GOSDBS nanocomposite. In addition, the frequency-sweep modulus studies using modulus master curves (**Figure 7**) revealed the extremely improved mechanical characteristics of this nanocomposite at high frequencies, compared to the PS sample. This confirms the formation of a high extent of interactions between GO nanosheets and the polysulfide matrix in the structure of the nanocomposite.

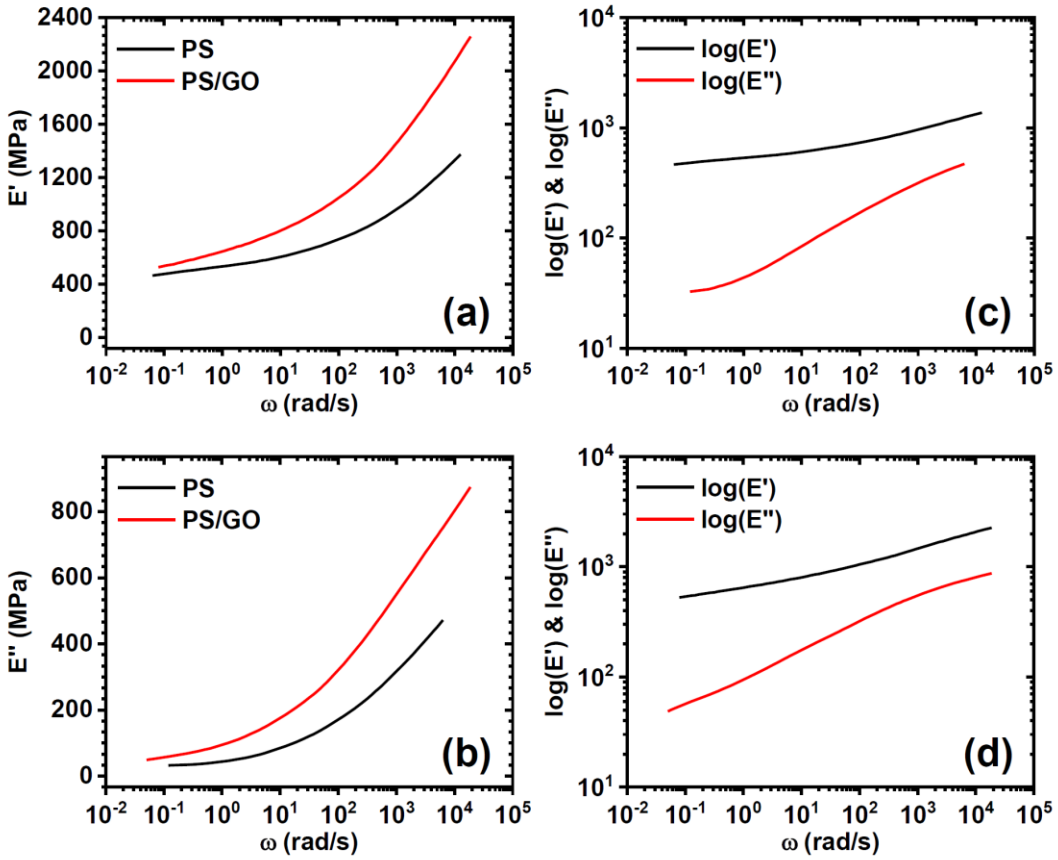

Figure 7. Frequency-sweep dynamic-mechanical behavior of samples: (a) storage modulus (E') and (b) loss modulus (E") master curves of samples (see Supporting Information for complete master curves) as well as comparative log(E') and log(E") curves of (c) PS and (d) PS/GO samples

It should be noted here that, although the content of loaded GO nanosheets in this study was very low (lower than the percolation threshold of the system), the electrical conductivity of the PS/GO nanocomposite was much lower than what we expected for this system. Two possible reasons can be considered: (i) high degree of GO aggregation in the structure of the

nanocomposite and (ii) the low electrical conductivity of GO nanosheets. GO nanosheets presented an exfoliated morphology in the structure of the fabricated PS/GO nanocomposite electrode. The intercalation of polysulfide macromolecules into the interlayer spacing of GO nanosheets resulted in the exfoliation of nanosheets and the formation of a perfectly dispersed morphological state for the PS/GO nanocomposite. Such a morphology can be considered as the main reason for the aforementioned improved mechanical and structural properties. However, as discussed earlier, in addition to GO nanosheets/polysulfide interactions and the morphological state of nanosheets, the molecular structure and carrier conduction of nanosheets are main factors affecting the electrical characteristics of the system.

The observed enhanced mechanical and electrical characteristics of the PS/GO nanocomposite can be easily related to the morphological state of GO nanosheets in the structure of this nanocomposite (**Figure 8**). The content of loaded-nanosheets plays a major role in the final properties of the system. At high nanosheet loading (contents higher than the percolation threshold of the system), the formation of an elastic network in the structure of nanocomposites affects almost all properties of these materials [37]. The formation of the elastic network results in a change in the electrical conductivity mechanism of the system, as a conduction pathway forms in the structure of the nanocomposite. However, at low GO-loading contents (nanosheet contents lower than the percolation threshold), the specific surface area of loaded nanosheets, as well as the nanosheet/polymer interface, control the final electronic properties of the system.

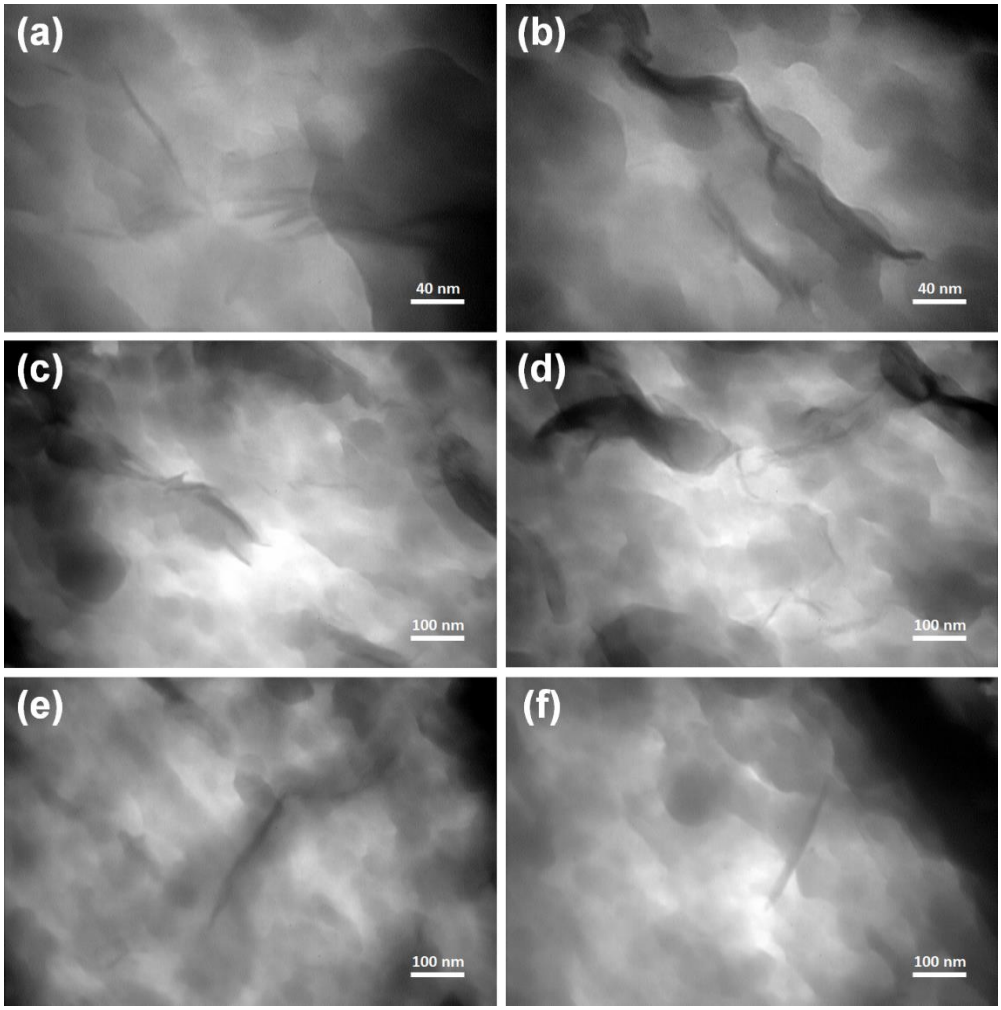

Figure 8. Morphological state of the fabricated nanocomposite electrode: TEM images of the molded PS/GO nanocomposite

As discussed earlier, in this study only 1 wt.% of GO nanosheets were incorporated into the structure of the nanocomposite, to make the role of nanosheet structure more clear. At such a low loading, the possibility of the formation of an elastic GO network in the structure of the nanocomposite is extremely low and therefore, properties of fabricated samples can completely represent the role of PS/GO interactions. However, even at such a low loading, the exfoliation of GO nanosheets can result in a dramatic enhancement in the properties of fabricated samples.

As depicted in Figure 8, GO nanosheets were perfectly dispersed in the PS/GO nanocomposite. Moreover, as discussed through the dynamic-mechanical studies (Figure 5 b), high interfacial

interactions were observed in the PS/GO interface. Although appropriate interactions between GO nanosheets and PS macromolecules due to oxygen functional groups on basal plane and edges of GO nanosheets favors the flexibility and mechanical properties of the system, the low electrical conductivity of GO nanosheets (1.75×10^{-5} S/m [38]) acts as a limitation for charge carrier transport in the nanocomposite electrode. This may affect the electrochemical performance of synthesized electrodes for Li-battery applications.

The cyclic voltammograms of PS and PS/GO electrodes at 1st, 5th, 10th, and 20th cycles between 0.5 and 4 V were presented in **Figure 9 (a and b)**. The redox behavior of both electrodes were very similar, with respect to the curve shape, peak position, current intensity, and curve evolution with the number of cycles. In the first cathodic sweep, both samples presented two shoulder peaks at 3 and 1 V. Moreover, in the subsequent oxidation sweep, two broad oxidation peaks were observed at 1.4 and 2.14 V for both electrodes. During the next five cycles, the voltammograms became stable with a clear shift in the peaks' positions and intensities. The reductive shoulder at 3V shrunk, whereas the shoulder at 1 V shifted to a higher potential of 1.31 V. A clear new reductive shoulder was also observed at 2V. The position of oxidation peaks remained almost unchanged through fifth cycle, and only an intensity change was observed for these peaks.

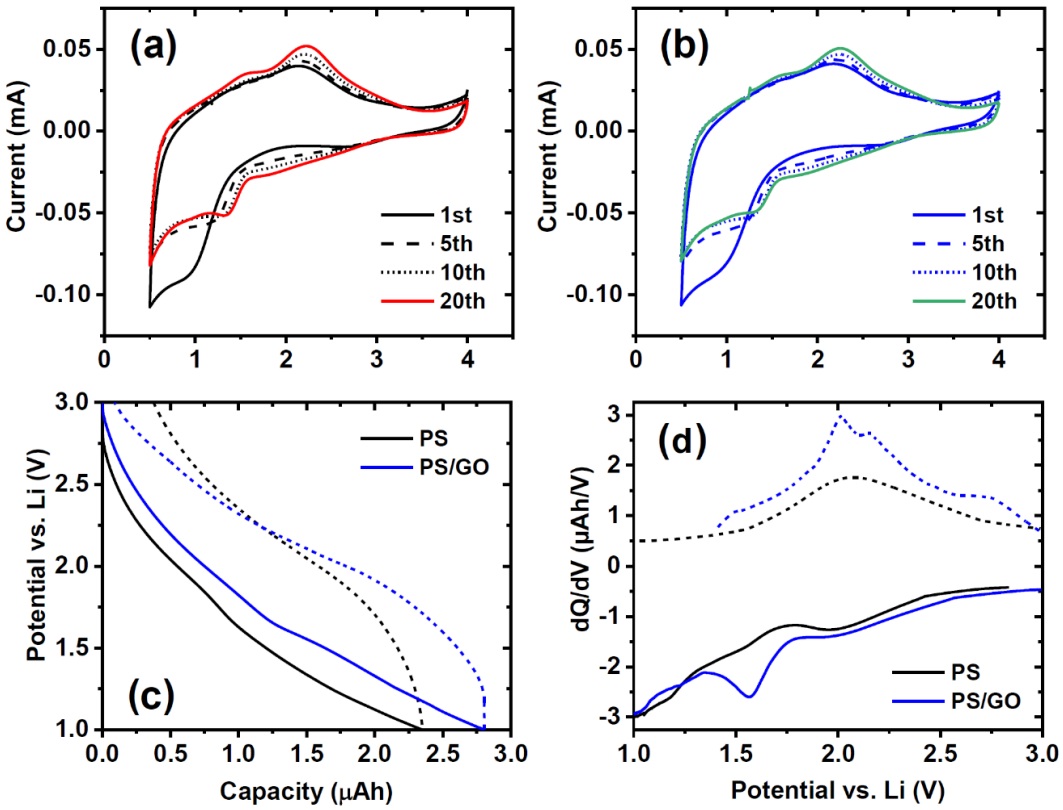

Figure 9. Cyclic voltammograms of samples: CV curves of (a) PS and (b) PS/GO samples recorded at a scan rate of 10 mV/s for cycles 1, 5, 10, and 20, (c) galvanostatic discharge (solid) and charge (dashed) plots as well as (d) corresponding differential-capacity plots for PS and PS/GO samples at a constant current of 0.5μA

Due to the complex nature of polysulfide electrochemistry, a complete study for an unequivocal identification of these peaks is required, which is beyond the scope of this preliminary study. However, according to the literature [9, 16], we speculate that the reductive and oxidative peak pairs at 2 and 2.14 V (vs. Li) correspond to the reversible depolymerization of di- or tri-thiolate lithium salts and re-polymerization of such complexes to disulfides, respectively. It is noteworthy that since the chemical nature of synthetic polysulfides reported in the literature for electrode applications, a comparison between results presented in this work for a polymeric organodisulfide electrode with a specific molecular weight and results presented in the literature for different polysulfides with dissimilar perceptions of a polymeric material might be deceptive.

Constant-current charge/discharge behavior (0.5 µA) for both PS and PS/GO samples were studied to assess the application potential of fabricated electrodes in rechargeable batteries. Figure 9 c and d present the voltage-capacity and the corresponding differential capacity plots for PS-Li (black) and PS/GO-Li (blue) cells, respectively. The Coulombic efficiencies of PS/GO-Li and PS-Li cells were 97% and 83%, respectively, which demonstrate the excellent reversibility of the (de)lithiation at the working electrodes in accordance with CV studies. The differential-capacity signature of electrodes (Figure 9 d) reconfirms the redox behavior discussed through CV studies. Two reductive peaks were clearly observed at 1.97 and 1.54 V. The observed oxidation trend in the differential-capacity curve of the PS/GO sample (Figure 6 d, dashed blue line) suggests that the broad oxidation peak cantered at 2V vs. Li (Figure 6 a) was a convolution of two close peaks at 2.03 and 2.15 V vs. Li. Moreover, a new oxidation peak was observed at 2.74 V vs. Li with the incorporation of GO nanosheets. It is noteworthy that the high resolution of redox peaks in differential-capacity plots (compared to CV plots) could be attributed to the fact that the current used in galvanostatic tests was very low.

Unambiguously, an increase in the ratio of sulfur/carbon atoms in the backbone of polysulfide electrodes can result in an enhancement in the storage potential of this class of electrodes. However, as discussed earlier, a decrease in the number of carbon atoms in the polymer backbone can reduce the electronic conductivity of the system. On the other hand, neither electrodes, nor the electrolyte used here, were optimized for battery tests. A method to reach a larger electrode/electrolyte interface can be the introduction of porosity in the structure of the electrode. A thin porous electrode with a high surface area is essential to leverage the full capacity of this system for battery applications, as confirmed by our initial results (not included here). Therefore, in our upcoming studies, we plan to address these aspects: the incorporation of graphene nanosheets (instead of GO nanosheets) in the structure of a flexible polysulfide

with a higher sulfur/carbon atomic ratio in the polymer backbone, and the introduction of porosity in the microstructure of polysulfide-based nanocomposite electrodes.

4. Conclusions

In summary, the structural, dynamic-mechanical, electrical and electrochemical properties of the crude polyethylene disulfide and polyethylene disulfide/GO nanocomposites synthesized using the interfacial polymerization technique were studied. The crude polyethylene disulfide presented a T_g of -10 °C and high storage moduli of 1492 and 98 MPa at - 45 °C and 25 °C, respectively. When only 1 wt.% GO nanosheets were incorporated, the T_g of the sample increased to -4.5 °C and clear variations in both intensity and position of the damping peak were observed, suggesting the formation of interactions between GO nanosheets and PS. These interactions resulted in an increase in the storage modulus of the sample to 115 MPa at room temperature (25 °C). The electrical conductivity of all fabricated samples were in the range of 10^{-4}-10^{-7} S/m through a wide range of frequencies (10-10^6 Hz), which is much higher than the electrical conductivity of the elemental sulfur (0.5×10^{-27} S/m). Due to the limited electrical conductivity of GO nanosheets, the GO-loaded nanocomposite presented only a slightly improved electrical conductivity compared to other samples. High Coulombic efficiencies of 97% and 83% were achieved for the PS and their GO-based nanocomposite electrodes in Li cells, respectively. Our results suggest that, although the concept of flexibility can be introduced to Li-batteries with polyethylene disulfide electrodes, a better in-depth understanding of design and engineering of both the matrix and the reinforcing agent, together with the optimization of the electrode formulation and microstructure are essential to reach a stable standalone flexible electrode with a high capacity and high stability.

Supporting Information

FTIR peak assignments, FTIR spectra of as-synthesized nanocomposites, TEM images of as-synthesized PS/GO nanocomposite, Time-temperature superposition data, TGA results of samples under N_2 atmosphere.

Data availability

The raw data required to reproduce these findings are available to download from [INSERT PERMANENT WEB LINK(s)]. The processed data required to reproduce these findings are available to download from [INSERT PERMANENT WEB LINK(s)].

References

[1] J. Zhu, P. Zhu, C. Yan, X. Dong, X. Zhang, Recent progress in polymer materials for advanced lithium-sulfur batteries, Prog. Polym. Sci. 90 (2019) 118-163.

[2] M. Arslan, B. Kiskan, E.C. Cengiz, R. Demir-Cakan, Y. Yagci, Inverse vulcanization of bismaleimide and divinylbenzene by elemental sulfur for lithium sulfur batteries, Eur. Polym. J. 80 (2016) 70-77.

[3] S.-R. Deng, L.-B. Kong, G.-Q. Hu, T. Wu, D. Li, Y.-H. Zhou, Z.-Y. Li, Benzene-based polyorganodisulfide cathode materials for secondary lithium batteries, Electrochim. Acta 51(13) (2006) 2589-2593.

[4] X. Liu, A. Wang, S. Wang, X. Liu, J. Chen, H. Xu, Q. Zeng, L. Zhang, A Hyperbranched Disulfide Polymer as Cathode Material for Lithium-Ion Batteries, J. Electrochem. Soc. 165(7) (2018) A1297-A1302.

[5] D. Han, B. Zhang, M. Xiao, P. Shen, S. Wang, G. Chen, Y. Meng, Polysulfide rubber-based sulfur-rich composites as cathode material for high energy lithium/sulfur batteries, Int. J. Hydrogen Energy 39(28) (2014) 16067-16072.

[6] S. Huang, R. Guan, S. Wang, M. Xiao, D. Han, L. Sun, Y. Meng, Polymers for high performance Li-S batteries: Material selection and structure design, Prog. Polym. Sci. 89 (2019) 19-60.

[7] M. Liu, Novel Solid Redox Polymerization Electrodes: All-Solid-State, Thin-Film, Rechargeable Lithium Batteries, J. Electrochem. Soc. 138(7) (1991) 1891-1895.

[8] S.J. Visco, M. Liu, M.B. Armand, L.C. de Jonghe, Solid Redox Polymerization Electrodes and Their Use in All-Solid-State Batteries, Mol. Cryst. Liq. Cryst 190(1) (1990) 185-195.

[9] S. Visco, M. Liu, M. Doeff, Y. Ma, C. Lampert, L. Dejonghe, Polyorganodisulfide electrodes for solid-state batteries and electrochromic devices, Solid State Ion. 60(1-3) (1993) 175-187.

[10] J.J. Griebel, R.S. Glass, K. Char, J. Pyun, Polymerizations with elemental sulfur: A novel route to high sulfur content polymers for sustainability, energy and defense, Prog. Polym. Sci. 58 (2016) 90-125.

[11] L. Sun, S. Gao, X. Gui, L. Liu, K. Xu, H. Liu, Renewable sulfur- and monoterpenes-derived polysulfides as functional crosslinker for epoxy thermosets, Eur. Polym. J. 123 (2020) 109440.

[12] E.-K. Bang, S. Ward, G. Gasparini, N. Sakai, S. Matile, Cell-penetrating poly(disulfide)s: focus on substrate-initiated co-polymerization, Polymer Chemistry 5(7) (2014) 2433.

[13] A. Pirayesh, M. Salami-Kalajahi, H. Roghani-Mamaqani, F. Najafi, Polysulfide Polymers: Synthesis, Blending, Nanocomposites, and Applications, Polymer Reviews 59(1) (2018) 124-148.

[14] A. Allahbakhsh, A.H. Haghighi, M. Sheydaei, Poly(ethylene trisulfide)/graphene oxide nanocomposites, J. Therm. Anal. Calorim. 128(1) (2016) 427-442.

[15] A.V. Tobolsky, W.J. MacKnight, M. Takahashi, Relaxation of Disulfide and Tetrasulfide Polymers, J. Phys. Chem. 68(4) (1964) 787-790.

[16] M.M. Doeff, The Use of Polydisulfides and Copolymeric Disulfides in the Li/PEO/SRPE Battery System, J. Electrochem. Soc. 139(8) (1992) 2077-2081.

[17] M. Sheydaei, A. Allahbakhsh, A.H. Haghighi, A. Ghadi, Synthesis and characterization of poly(methylene disulfide) and poly(ethylene disulfide) polymers in the presence of a phase transfer catalyst, J. Sulfur Chem. 35(1) (2013) 67-73.

[18] A.H. Haghighi, M. Sheydaei, A. Allahbakhsh, M. Ghatarband, F.S. Hosseini, Thermal performance of poly(ethylene disulfide)/expanded graphite nanocomposites, J. Therm. Anal. Calorim. 117(2) (2014) 525-535.

[19] E.M. Fettes, J.S. Jorczak, Polysulfide Polymers, Ind. Eng. Chem. Res. 42(11) (1950) 2217-2223.

[20] J.S. Jorczak, E.M. Fettes, Polysulfide Liquid Polymers, Ind. Eng. Chem. Res. 43(2) (1951) 324-328.

[21] K. Kishore, K. Ganesh, Polymers containing disulfide, tetrasulfide, diselenide and ditelluride linkages in the main chain, Polymer Synthesis/Polymer Engineering, Springer Berlin Heidelberg, Berlin, Heidelberg, 1995, pp. 81-121.

[22] M. Hayashi, Y. Shiro, H. Murata, Molecular Vibrations and Structures of Polyalkyl Polysulfides. II. Polyethylene Disulfide, Bull. Chem. Soc. Jpn. 39(9) (1966) 1861-1866.

[23] Y. Zhang, L. Shao, D. Dong, Y. Wang, Enhancement of water and organic solvent resistances of a waterborne polyurethane film by incorporating liquid polysulfide, RSC Advances 6(21) (2016) 17163-17171.

[24] E.J. Goethals, Sulfur-Containing Polymers, Journal of Macromolecular Science, Part C: Polymer Reviews 2(1) (1968) 73-144.

[25] M. Hayashi, Y. Shiro, H. Murata, Molecular Vibrations and Structures of Polyalkyl Polysulfides. I. Polymethylene Disulfide, Bull. Chem. Soc. Jpn. 39(9) (1966) 1857-1861.

[26] H. Yi, M. Jiang, D. Huang, G. Zeng, C. Lai, L. Qin, C. Zhou, B. Li, X. Liu, M. Cheng, W. Xue, P. Xu, C. Zhang, Advanced photocatalytic Fenton-like process over biomimetic hemin-Bi2WO6 with enhanced pH, Journal of the Taiwan Institute of Chemical Engineers 93 (2018) 184-192.

[27] A.M. Usmani, Chemistry and Technology of Polysulfide Sealants, Polym.-Plast. Technol. Eng. 19(2) (2006) 165-199.

[28] R.S. Lakes, High Damping Composite Materials: Effect of Structural Hierarchy, J. Compos. Mater. 36(3) (2016) 287-297.

[29] A. Allahbakhsh, F. Noei Khodabadi, F.S. Hosseini, A.H. Haghighi, 3-Aminopropyl-triethoxysilane-functionalized rice husk and rice husk ash reinforced polyamide 6/graphene oxide sustainable nanocomposites, Eur. Polym. J. 94 (2017) 417-430.

[30] D.-W. Wang, Q. Zeng, G. Zhou, L. Yin, F. Li, H.-M. Cheng, I.R. Gentle, G.Q.M. Lu, Carbon–sulfur composites for Li–S batteries: status and prospects, J. Mater. Chem. A 1(33) (2013) 9382-9394.

[31] X. Li, J. Liang, X. Li, C. Wang, J. Luo, R. Li, X. Sun, High-performance all-solid-state Li–Se batteries induced by sulfide electrolytes, Energy Environ. Sci. 11(10) (2018) 2828-2832.

[32] M. Amaike, T. Iihama, Chemical polymerization of pyrrole with disulfide structure and the application to lithium secondary batteries, Synth. Met. 156(2-4) (2006) 239-243.

[33] J. Li, H. Zhan, L. Zhou, S. Deng, Z. Li, Y. Zhou, Aniline-based polyorganodisulfide redox system of high energy for secondary lithium batteries, Electrochem. Commun. 6(6) (2004) 515-519.

[34] L.J. Xue, J.X. Li, S.Q. Hu, M.X. Zhang, Y.H. Zhou, C.M. Zhan, Anthracene based organodisulfide positive active materials for lithium secondary battery, Electrochem. Commun. 5(10) (2003) 903-906.

[35] A.N. Papathanassiou, I. Sakellis, J. Grammatikakis, Universal frequency-dependent ac conductivity of conducting polymer networks, Appl. Phys. Lett. 91(12) (2007) 122911.

[36] B.M. Greenhoe, M.K. Hassan, J.S. Wiggins, K.A. Mauritz, Universal power law behavior of the AC conductivity versus frequency of agglomerate morphologies in conductive carbon nanotube-reinforced epoxy networks, J. Polym. Sci., Part B: Polym. Phys. 54(19) (2016) 1918-1923.

[37] Y. Li, Y.A. Samad, K. Polychronopoulou, S.M. Alhassan, K. Liao, Highly Electrically Conductive Nanocomposites Based on PolymerInfused Graphene Sponges, Scientific Reports 4(1) (2014).

[38] R. Pasricha, S. Gupta, A.K. Srivastava, A Facile and Novel Synthesis of Ag–Graphene-Based Nanocomposites, Small 5(20) (2009) 2253-2259.